Supplementary Information

Burst pressure of passive stop valves and flow control theory to dispense the liquid into microchambers

As illustrated in Fig. S1, the liquid is pinned at the back edge of the convex structure of the passive valves owing to surface-tension forces. The theoretical burst pressures for valves S_1 and S_2 are delineated as follows [1,2]:

$$P_1 = -\gamma\left(\frac{cos\left(min\left(\theta_m+\beta,180°\right)\right)+cos\theta_m}{g_1+r_1(1-\cos\beta)}+\frac{cos\theta_m+cos\theta_f}{H}\right)\#(1)$$

$$P_2 = -\gamma\left(\frac{2cos\left(min\left(\theta_m+\beta,180°\right)\right)}{g_2+r_2(1-\cos\beta)}+\frac{cos\theta_m+cos\theta_f}{H}\right)\#(2)$$

where g_1 (43.7 μm) and g_2 (23.4 μm) represent the gap lengths of valves S_1 and S_2, respectively. H denotes the height of the microchannel, ϑ_m is the contact angle of water on the surfaces of the top and sidewalls of the microchannel at a narrow gap (i.e., ϑ_m = 108° for PDMS), ϑ_f is the contact angle of water on the bottom surface of the microchannel (namely, ϑ_f = 102° for silicone-based adhesive double-sided tape), and γ is the surface tension of the liquid (γ = 0.073 N/m for water). r_1 (6.9 μm) and r_2 (6.0 μm) are the radii of the passive valves S_1 and S_2, respectively. β is the angle between the direction perpendicular to the longitudinal direction of the microchannel and the position of the liquid–air meniscus, which is pinned at the corner of the convex structure.

During the dispensing process into multiple microchambers, the potential number of microchambers that can be filled and the maximum permissible flow rate can be estimated using our proposed sequential liquid dispensing theory, which is expressed by the following equation [2]:

$$P_2 > P_1 + \Delta P(L_1) + \Delta P(L_2) + \Delta P(L_3)\#(3)$$

where $\Delta P(L_1)$, $\Delta P(L_2)$, and $\Delta P(L_3)$ are the pressure differences required to move a liquid through microchannels of lengths L_1, L_2, and L_3, respectively. The theoretical pressure drop $\Delta P(L)$ due to flow resistance in a rectangular microchannel is expressed by [3]:

$$\Delta P(L) = Q \times \frac{12\eta L}{H^3 W}\left(1-0.630\frac{H}{W}\right)^{-1}\#(4)$$

where W, H, and L represent the microchannel's width, height, and length, respectively; η is the dynamic viscosity of the liquid (η = 1 mPa·s for water), and Q is the volumetric flow rate. The lengths of the microchannels, L_1 = 1.47 mm, L_2 = 0.8 mm, and L_3 = 1.0 mm, are specified as depicted in Fig. S1.

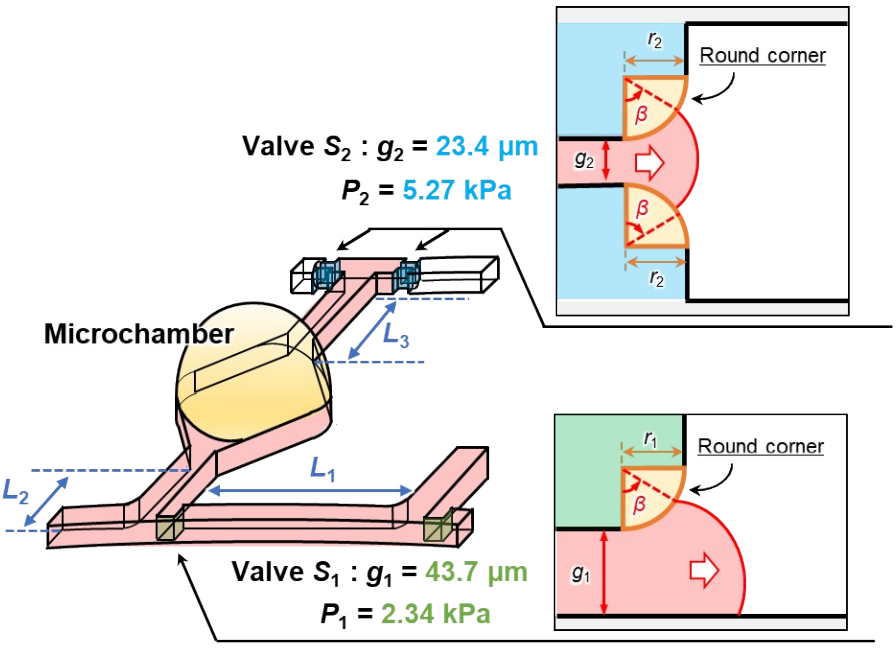

Fig. S1 Detailed design of a microchamber integrated with a passive valve system, including a single-faced stop valve (temporary stop valve S_1) and a set of two double-faced stop valves (permanent stop valves S_2).

References

1 D. Natsuhara, R. Saito, H, Aonuma, T. Sakurai, S. Okamoto, M. Nagai, H. kanuka and T. Shibata, A method of sequential liquid dispensing for the multiplexed genetic diagnosis of viral infections in a microfluidic device, *Lab Chip*, 2021, **21**(24), 4779-4790, DOI: 10.1039/d1lc00829c.

2 D. Natsuhara, S. Misawa, R. Saito, K. Shirai, S. Okamoto, M. Nagai, M. Kitamura and T. Shibata, A microfluidic diagnostic device with air plug-in valves for the simultaneous genetic detection of various food allergens, *Sci. Rep.*, 2022, **12**, 12852, DOI: 10.1038/s41598-022-16945-2.

3 E. Yildirim, S. J. Trietsch, J. Joore, A. van den Berg, T. Hankemeiera and P. Vulto, Phaseguides as tunable passive microvalves for liquid routing in complex microfluidic networks, *Lab Chip*, 2014, **14**(17), 3334-3340, DOI: 10.1039/C4LC00261J.

Supplementary figures

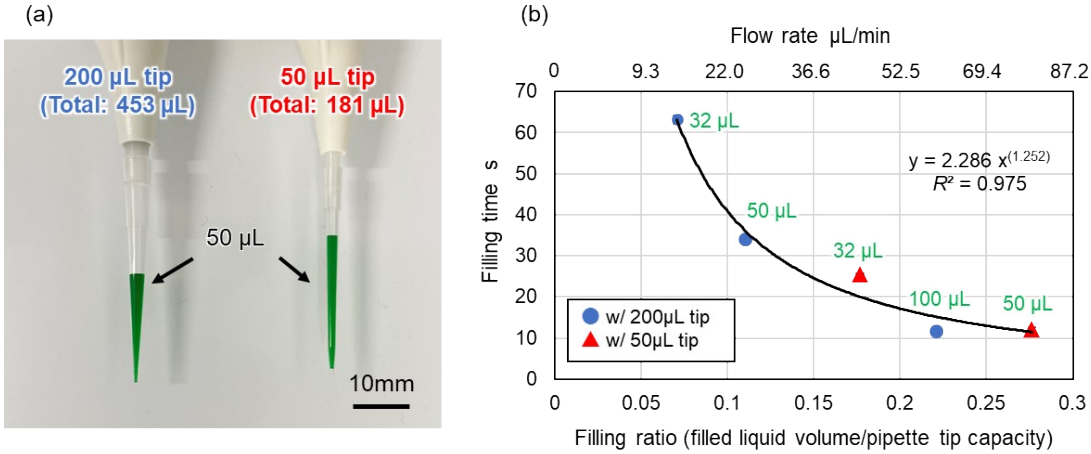

Fig. S2 Experimental results demonstrating the performance of the electric pipette for liquid dispensing. (a) Photographs show a 200-µL pipette tip (with a maximum capacity of 453 µL) and a 50-µL pipette tip (with a maximum capacity of 181 µL), both filled with 50 µL of green-colored water, resulting in filling ratios of 0.11 and 0.28, respectively. (b) Filling time required for dispensing the liquid into five microchambers as a function of the filing ratio (defined as the ratio of the volume of filled liquid to the capacity of the pipette tip). The flow rate is an estimated value calculated from the filling time, and the numbers in the figure represent the volume of the filled liquid in the pipette tip.

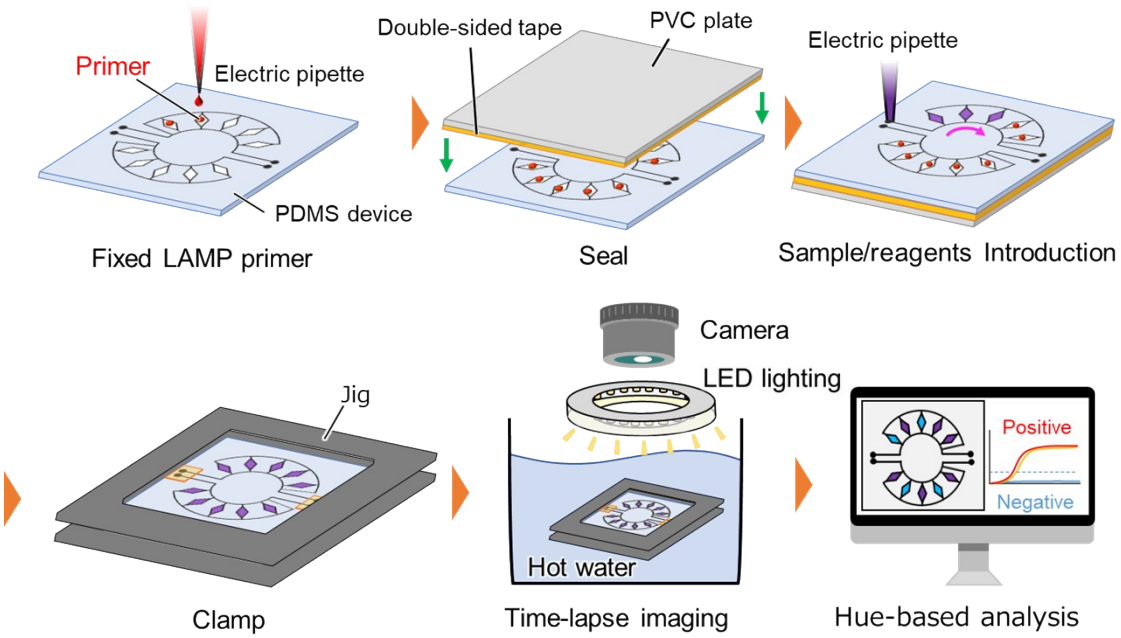

Fig. S3 Operating procedure for the multiplexed colorimetric LAMP detection of nucleic-acid targets using the microfluidic-based quantitative analysis system.

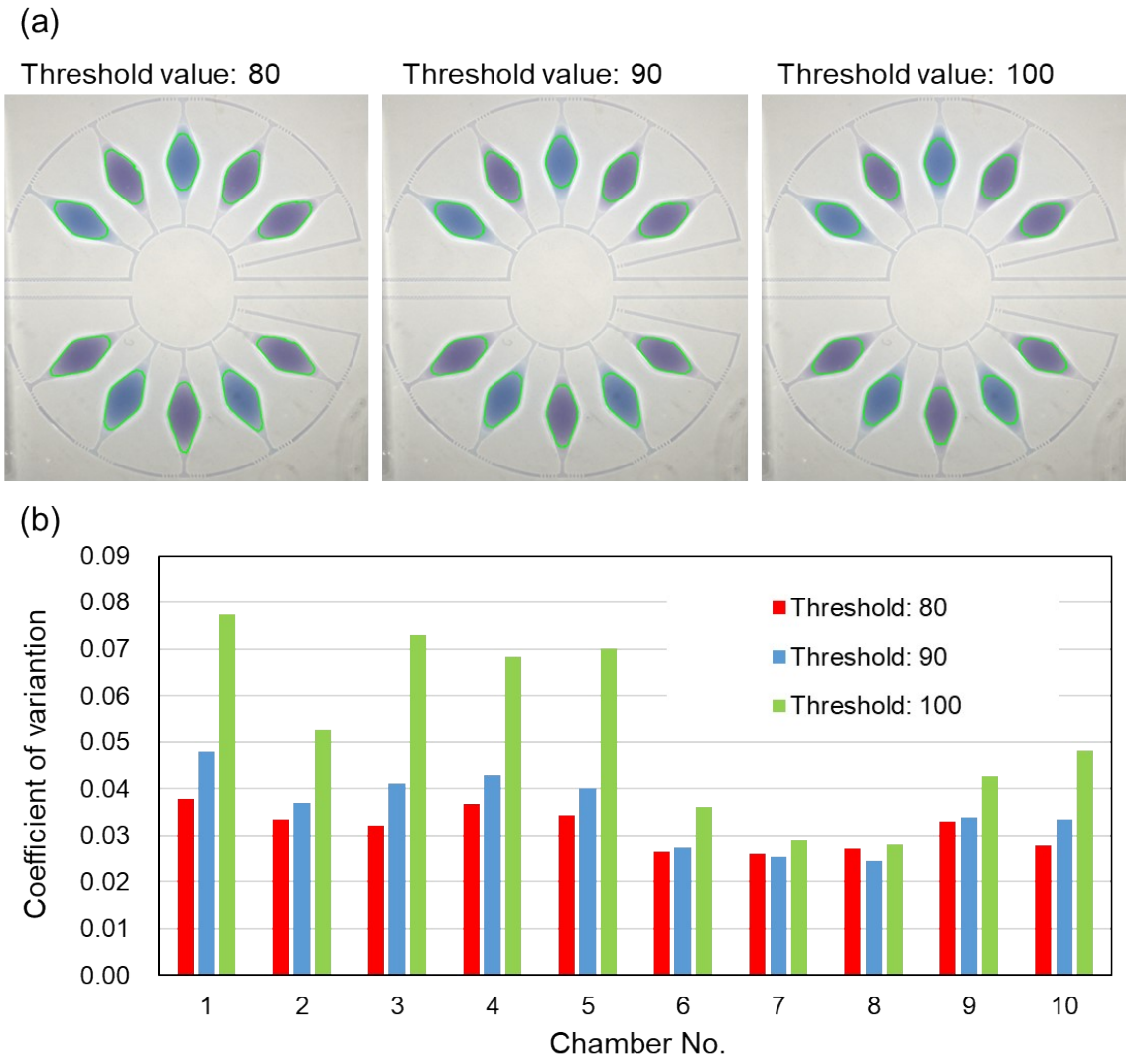

Fig. S4 Influence of the threshold value in binarization processing on the identification accuracy of reaction chambers. (a) Green circular areas in images represents the recognized regions using threshold values of 80, 90, and 100. (b) Coefficient of variations in the area of recognized chamber regions during LAMP assays for 60 min.

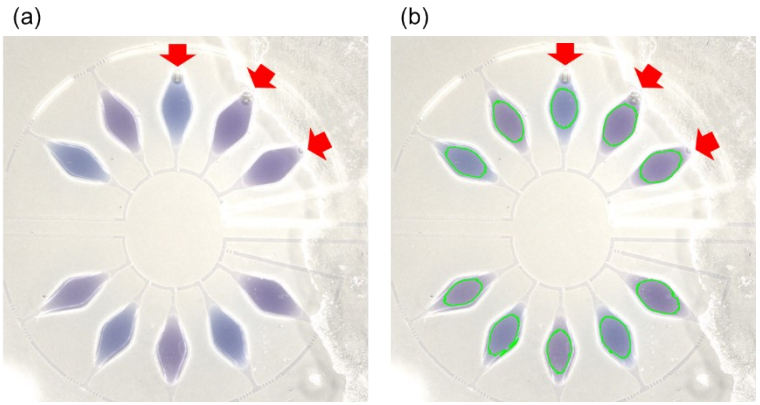

Fig. S5 Influence of air bubbles present in the microchambers on the recognition of chamber regions. (a) Photograph of microchambers containing air bubbles, indicated by red arrows. (b) Chamber regions after image processing, resulting in the removal of unexpected air bubbles generated within the chambers during the LAMP assay. Green circular areas in the images represents the recognized regions.

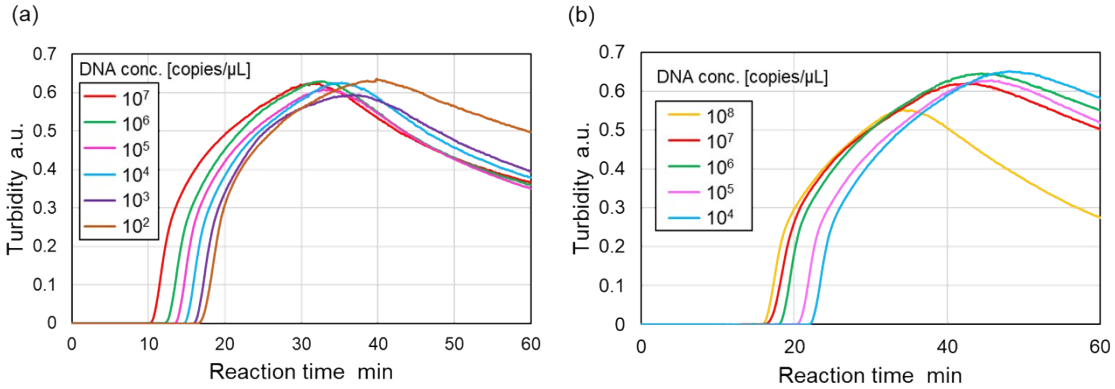

Fig. S6 Experimental results showing the turbidity measurements of conventional LAMP assays using a commercially available turbidimeter. (a) DNA amplification curves for the detection of HSV-1 samples (10^2–10^7 copies/µL). (b) DNA amplification curves for the detection of HSV-2 samples (10^4–10^8 copies/µL).

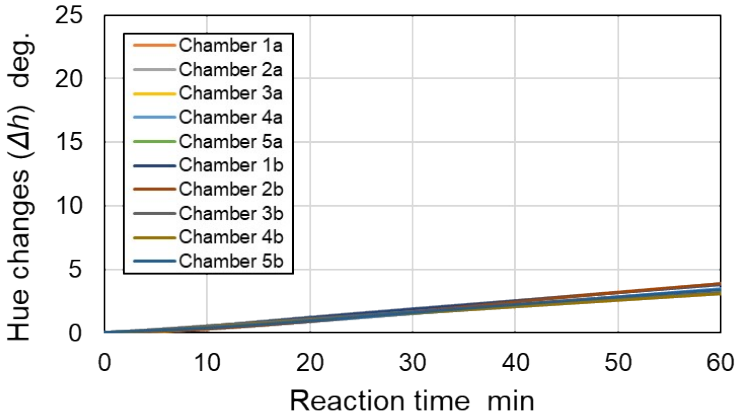

Fig. S7 Experimental demonstration of the LAMP assay with a template-free sample as a negative control.

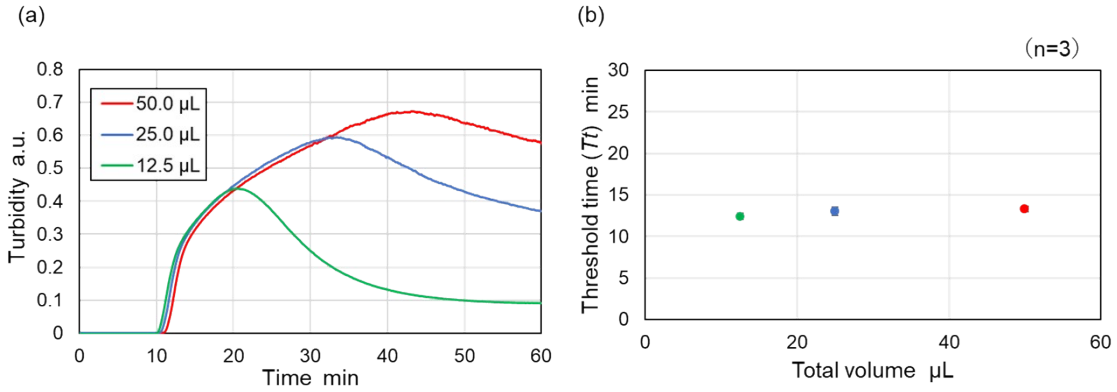

Fig. S8 Influence of the sample/LAMP reagents volume on LAMP reactions conducted using a commercially available turbidimeter. (a) DNA amplification curves for HSV-1 samples (10^7 copies/µL) with reaction volumes of 12.5 µL, 25.0 µL, and 50.0 µL. (b) Mean threshold time (*Tt*) against the reaction volume of the mixture (n=3).

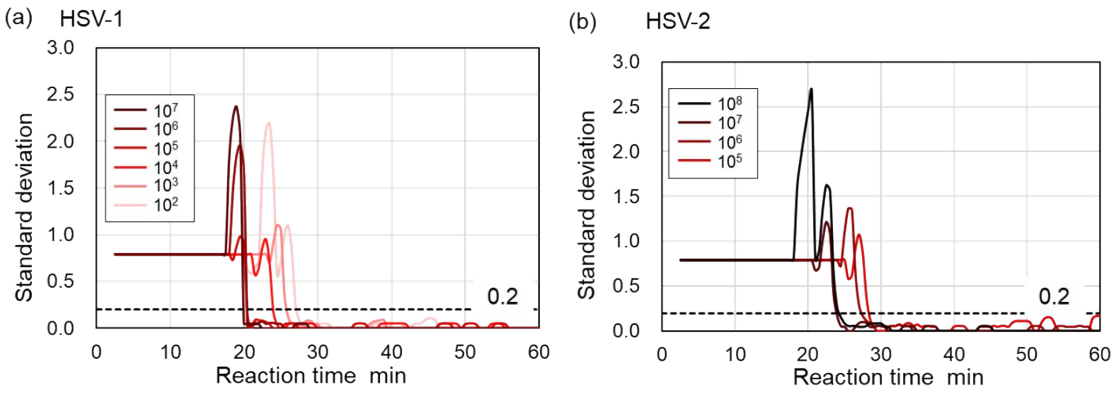

Fig. S9 Temporal variation of the SD_x to determine the convergence time (Tt) for (a) HSV-1 (10^2–10^7 copies/µL) and (b) HSV-2 (10^5–10^8 copies/µL) over a duration of 60 min.

Supplementary tables

Table S1 Components and volume used for colorimetric LAMP assays in the microfluidic device

Component	Concentration	Volume (μL)
2× Reaction mixture	–	18.75
Bst DNA polymerase	8 U/μL	1.5
DNA template	10^3–10^8 copies/μL for HSV-1 10^9–10^6 copies/μL for HSV-2	3.75
Primer [a]	FIP 30 pmol BIP 30 pmol F3 5 pmol B3 5 pmol LF 15 pmol LB 15 pmol	(0.5)
Hydroxynaphthol blue	4.2 mM	1.34
Distilled water	–	12.16
Total		37.5 [b]

[a] Primer sets were pre-spotted and dried in each reaction chamber at 80 ℃ for 3 min.

[b] Total volume does not include the volume of the primer.

Table S2 Components and volume used for conventional off-chip LAMP assays performed in a 0.2-mL PCR tube using a real-time turbidimeter

Component	Concentration	Volume (μL)
2× Reaction mixture	–	12.5
Bst DNA polymerase	8 U/μL	1.0
DNA template	10^3–10^8 copies/μL for HSV-1 10^9–10^6 copies/μL for HSV-2	2.5
Primer	FIP 30 pmol BIP 30 pmol F3 5 pmol B3 5 pmol LF 15 pmol LB 15 pmol	4.0
Distilled water	–	5.0
Total		25.0

Table S3 Comparison of *Tt* values derived from the fitting curve of the complete dataset for HSV-1 detection after 60 min and the elapsed time (t_x) at which *Tt* values stabilized. *Tt* and t_x are presented as mean ± standard deviation, based on four experimental replicates.

DNA [copies/µL]	10^2	10^3	10^4	10^5	10^6	10^7
Tt [min]	20.7 ± 0.4	19.6 ± 0.9	18.7 ± 0.4	15.8 ± 0.9	14.3 ± 0.4	13.1 ± 0.7
t_x [min]	27.1 ± 0.3	25.8 ± 1.9	25.6 ± 1.6	23.8 ± 3.8	24.0 ± 4.0	24.1 ± 3.9
t_x/Tt	1.31	1.32	1.37	1.51	1.66	1.86

Table S4 Comparison of *Tt* values derived from the fitting curve of the complete dataset for HSV-2 detection after 60 min, and the elapsed time (t_x) at which *Tt* values stabilized. *Tt* and t_x are presented as mean ± standard deviation, based on four experimental replicates.

DNA [copies/µL]	10^5	10^6	10^7	10^8
Tt [min]	21.0 ± 0.9	20.1 ± 1.4	17.5 ± 0.3	16.5 ± 0.3
t_x [min]	27.6 ± 0.8	27.3 ± 1.7	25.5 ± 1.7	24.1 ± 0.3
t_x/Tt	1.31	1.36	1.46	1.46